 ISSN 0267-8179. DOI: 10.1002/jqs.3059

JQS Journal of Quaternary Science QRA Quaternary Research Association

Revisiting an arid LGM using fluvial archives: a luminescence chronology for palaeochannels of the Murrumbidgee River, south-eastern Australia

DANIELA MUELLER,[1,2]* ZENOBIA JACOBS,[3,4] TIM J. COHEN,[1,3] DAVID M. PRICE,[1] IVARS V. REINFELDS[1,5] and JAMES SHULMEISTER[6]

[1]GeoQuest Research Centre, School of Earth and Environmental Sciences, University of Wollongong, Wollongong, NSW, Australia
[2]Institute of Earth and Environmental Sciences, Albert-Ludwigs-Universität, Freiburg, Germany
[3]ARC Centre of Excellence for Australian Biodiversity and Heritage, University of Wollongong, Wollongong, NSW, Australia
[4]Centre for Archaeological Science, School of Earth and Environmental Sciences, University of Wollongong, Wollongong, NSW, Australia
[5]New South Wales Department of Industry - Water, Wollongong, NSW, Australia
[6]School of Earth and Environmental Sciences, the University of Queensland, St Lucia, Brisbane, QLD, Australia

Received 19 September 2017; Revised 7 June 2018; Accepted 14 June 2018

ABSTRACT: The Riverine Plain in south-eastern Australia contains numerous palaeochannels that are much larger than the present rivers and provide evidence about past hydrological conditions. Previous research suggested optima in fluvial activity both before and after the peak of the Last Glacial Maximum (LGM; 21 ± 3 ka), and, in some cases, throughout the LGM. In this study, we revisit palaeochannel remnants of the Gum Creek and Yanco palaeochannel systems along the Murrumbidgee River, which drains the high-elevation catchments of the Australian Alps in south-eastern Australia. We date fluvial and aeolian sediments using single-grain optically stimulated luminescence (OSL) and apply thermoluminescence (TL) dating to a subset of samples. We compare the OSL ages to new and previously published TL ages and investigate reasons for age discrepancies between these methods, possible effects of partial bleaching and other factors that may affect luminescence ages. We propose a new OSL-based chronology for the Gum Creek and Yanco palaeochannel systems and assign periods of enhanced fluvial activity for the Tombullen and Yanco phases to 41–29 and 29–18 ka, respectively. Importantly, we infer that conditions of increased sediment and water discharge persisted for the Murrumbidgee River at the time of the LGM.

KEYWORDS: palaeohydrology; quartz grains; riverine plain; single-grain OSL; TL.

Introduction

The Riverine Plain of south-eastern Australia (Fig. 1A) and its myriad of palaeochannels have been investigated since the mid-20th century (e.g. Butler, 1958; Langford-Smith, 1959; Pels, 1964; Schumm, 1968). This vast alluvial plain (77 000 km^2 in area) forms part of the Murray–Darling Basin (Brown and Stephenson, 1991) and contains important terrestrial archives that provide valuable evidence about past hydrological conditions (e.g. Langford-Smith, 1959; Butler, 1960; Pels, 1964; Schumm, 1968). Palaeochannels of major rivers, such as the Murrumbidgee, Lachlan and Goulburn rivers (Fig. 1B), are characterized by much larger channels, larger meander wavelengths and coarser bed material than observed at present (e.g. Bowler, 1978; Page and Nanson, 1996; Kemp and Rhodes, 2010). Such morphological and sedimentological differences between former and modern river systems are used as indicators of change to the hydrological and sediment regime, reflective of higher discharge due to changes in runoff volume, flood frequency and sediment supply (e.g. Harvey, 1969; Dury, 1976; Hickin, 1977; Williams, 1984; Bishop and Godley, 1994).

Previous studies of palaeochannel deposits along the Murrumbidgee River have suggested that more competent river systems (such as the Gum Creek and Yanco systems; Fig. 1C) were active before and after the global Last Glacial Maximum (LGM; 21 ± 3 ka; Mix *et al.*, 2001), and that the peak of the LGM was represented by 'a brief period of aridity and reduced fluvial activity' (Page *et al.*, 1996). In contrast, equivalent palaeochannel remnants of the Lachlan and Goulburn rivers (other tributaries within the MDB; Fig. 1B) were interpreted to have been shaped by discharge regimes that were active throughout the LGM (Bowler, 1978; Kemp *et al.*, 2017). While an absence of fluvial activity at the peak of the LGM was not reported for these sub-catchments, a reduced discharge has been suggested for the Lachlan River by Kemp and Rhodes (2010).

Regional pollen records suggest drier conditions during the LGM as indicated by an increase of herb taxa along the Great Dividing Range and its foothills (e.g. Singh and Geissler, 1985; Dodson and Wright, 1989; Williams *et al.*, 2006), whereas evidence at lakes Kanyapella, George, Mungo and Menindee (Fig. 1B) have led to ambiguous interpretations of palaeohydrological conditions for south-eastern Australia from high to highly fluctuating lake levels (e.g. Galloway, 1965; Coventry, 1976; Hope, 1983; Bowler *et al.*, 2003). These conflicting findings of enhanced aridity versus lake-full conditions during the LGM represent a longstanding conundrum in our understanding of palaeohydrological conditions of the region (e.g. Hesse *et al.*, 2004; Petherick *et al.*, 2013; Reeves *et al.*, 2013). This may be the result of different dating

*Correspondence: Daniela Mueller, [2]Institute of Earth and Environmental Sciences, as above.
E-mail: daniela.mueller@geologie.uni-freiburg.de

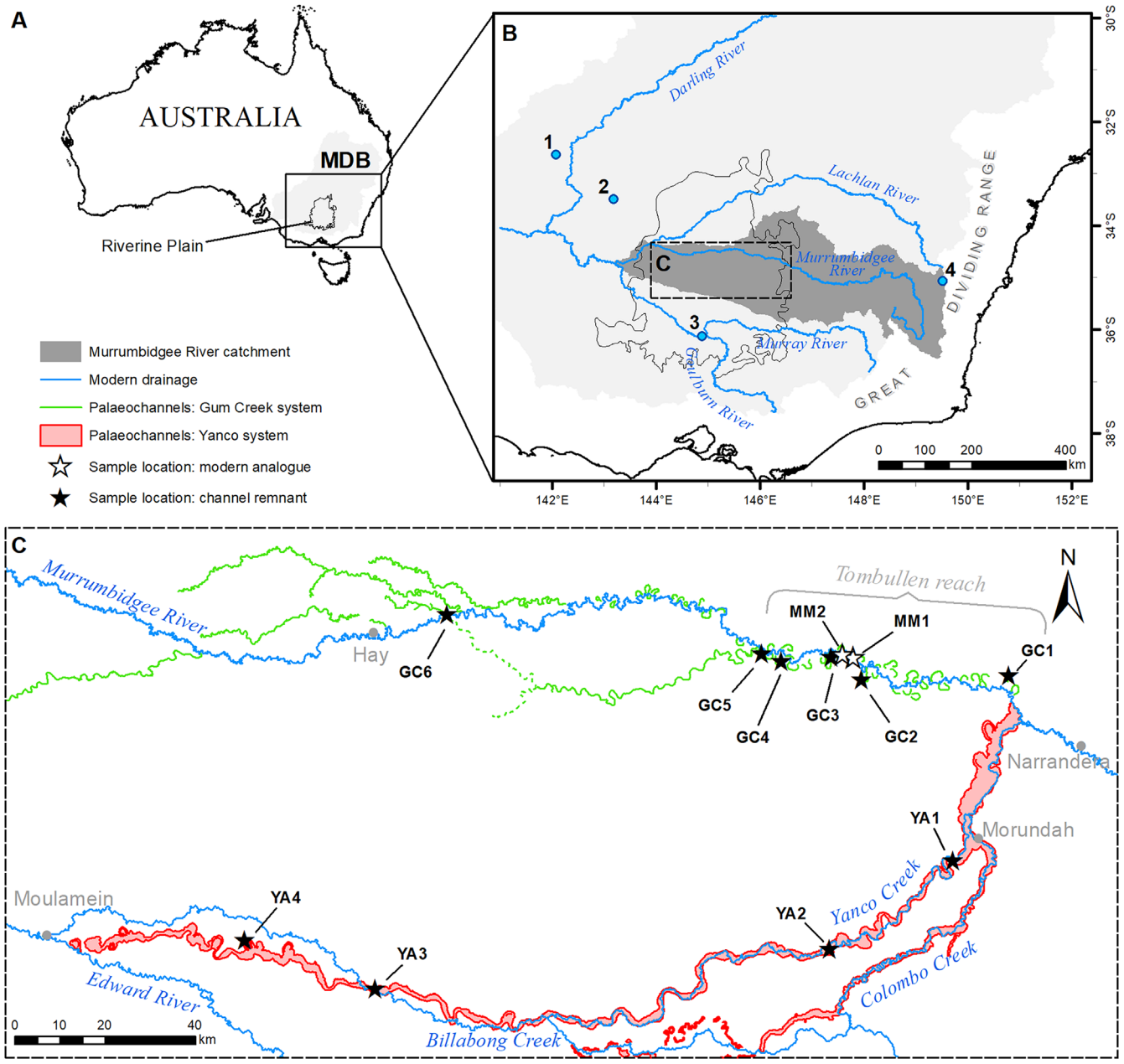

Figure 1. Overview of the Murrumbidgee River study area. **A**: Map of Australia showing the location of the Riverine Plain and Murray–Darling Basin (MDB). **B**: Major rivers of the Riverine Plain, river catchment area of the Murrumbidgee River and lake locations mentioned in the text (1: Menindee Lakes; 2: Lake Mungo; 3: Lake Kanyapella; 4: Lake George). **C**: Sample locations at the modern Murrumbidgee River and its two palaeochannel systems (Gum Creek and Yanco). [Colour figure can be viewed at wileyonlinelibrary.com].

techniques being applied [e.g. radiocarbon, and thermoluminescence (TL), optically stimulated luminescence (OSL)], resulting in chronologies with varying accuracy and precision, or could be the result of what palaeoenvironmental proxies have been used to infer past water balance.

While understanding that past water balance is crucial for the reconstruction of palaeoenvironments of a given region, it is also important to identify the presence or absence of regional arid and humid phases at a broader hemispheric scale. For example, changes in Southern Hemisphere atmospheric circulation have commonly been linked to local palaeohydrological conditions (Shulmeister *et al.*, 2004; Zhu *et al.*, 2014). The intensification or displacement of major circulation belts such as the Southern Westerly Winds have been directly linked to precipitation records derived from glacial and lacustrine records (Moreno *et al.*, 1999; Kaplan *et al.*, 2004; McCulloch *et al.*, 2005). Using unambiguous records of palaeorunoff from westerly-derived snow provides such an opportunity and is especially important for periods such as the LGM, which is considered to represent the last substantial period of climatic change during the late Quaternary (Braconnot *et al.*, 2012).

The aim of this study is, therefore, to evaluate the chronology of large palaeochannels. We revisit and date key sites of the Gum Creek and Yanco palaeochannel systems along the Murrumbidgee River using single-grain OSL dating of sedimentary quartz grains extracted from both fluvial and aeolian deposits. We also conduct TL dating on a subset of samples for direct comparison with the new single-grain OSL ages and with previous TL ages obtained for the same palaeochannel systems, presented in Page *et al.* (1996). This comparison is critical because it allows direct comparison of the two dating techniques and an assessment of the existing interpretations for the development of these palaeochannel systems based on chronologies that are almost entirely based on TL dating. We finally provide a revised chronology for the

late Pleistocene Gum Creek and Yanco palaeochannel systems and evaluate the presence or absence of enhanced fluvial activity during the LGM. A detailed palaeohydrological investigation of these palaeochannels and an assessment of the LGM water balance will be provided elsewhere.

Geological setting and study area

The Murrumbidgee River is a tributary of Australia's longest river system, the Murray–Darling, and originates in the temperate regions of the Great Dividing Range with its headwaters at elevations of up to ~2050 m above sea level (AHD) (Fig. 1B). It flows west onto the Riverine Plain, where it is characterized by a series of anabranches and its major distributary, Yanco Creek (Fig. 1C). At its confluence with the Murray River, the ~1600-km-long Murrumbidgee River drains a total area of 84 000 km^2 (Green *et al.*, 2011) with considerable areas (>6000 km^2) at elevations above 1000 m AHD (Geoscience Australia, 2011).

The large palaeochannels and billabongs are easily distinguishable from the smaller modern drainage system, especially on the Riverine Plain, a 77 000-km^2-wide, low-gradient, distributary fluvial system with mean elevations of ~100 m AHD. The plain is a ~400-m-thick depocentre of marine and terrestrial Cenozoic sediments (Brown and Stephenson, 1991) and its surface is characterized by ephemeral lakes, source-bordering dunes and an extensive network of coalescing floodplains and palaeochannels.

Two morphologically distinct palaeochannel systems – the Gum Creek and Yanco systems – have been identified and dated previously by Page *et al.* (1996). Based on the early TL chronology, the palaeochannels of the Gum Creek system (Fig. 1C) were thought to have been active 35–25 ka (Page *et al.*, 1996) and are preserved as a series of wide channel remnants, of lateral migrating character, close to the modern river. Former bankfull discharge capacities were estimated to exceed the present by four times (Page and Nanson, 1996). The Yanco system branches away from the modern river course downstream of Narrandera (Fig. 1C) and is characterized by even wider channels (4.5 times the discharge capacity of the modern channel; Page and Nanson, 1996), as well as distinct scroll bar patterns and source-bordering dunes, especially in the downstream reaches. Previously obtained TL ages from the Yanco palaeochannels indicated a phase of enhanced fluvial activity 20–13 ka (Page *et al.*, 1996) and a more recent study suggested, based on one additional multi-grain OSL age, that this phase extended until ~9 ka (Banerjee *et al.*, 2002).

Methods

Sampling for luminescence dating

We collected 33 samples from the Gum Creek and Yanco palaeochannel systems, source-bordering dunes and the modern channel. Six sites between Narrandera and Hay (five within the 'Tombullen reach' as defined by Page *et al.*, 1996) were chosen for assessment of the Gum Creek (GC) system (Fig. 1C). Four sites between Morundah and Moulamein were chosen for analysis of the Yanco system (YA) (Fig. 1C). In Table 1, samples are grouped according to the palaeochannel system from which they were collected and then ordered by site location. Also provided are the site coordinates and methods of sample collection; samples collected from the same core share a location code. Fig. 2 provides digital elevation models (DEMs) for each of the sample sites with sample locations indicated by stars and transects as lines.

Bedload deposits were targeted for dating as they represent the last time interval of channel activity. Dating of the channel fill, a proxy for when fluvial activity ceased, was not possible due to a lack of sand-sized grains for OSL dating and organic matter for radiocarbon dating. At seven locations (GC1-1, GC2-1, GC3-1, GC4-1, GC5-1, YA1-1, YA4-1; Figs. 1–3) drill cores were collected from palaeochannel depressions, where former bedload material was readily identifiable and sampled for dating. Fig. 3 shows cross-sections, core logs and OSL sample locations for all drill sites. At YA4 and GC2 additional cores were drilled along a transect from the palaeochannel meander *apex* through several palaeo-scroll bars (Fig. 2). Samples were also collected from pits or cut banks of the modern river at sites with laterally accreted deposits (YA2, YA3, GC6) (Fig. 2), from lunettes close to the channel remnants of the Gum Creek system (GC2-5, GC5-3), and a source-bordering dune of the Yanco system (YA4-2) (Fig. 2). Given that turbid flows with a high suspended load may not necessarily allow for bedload sediment to be sufficiently exposed to sunlight before deposition and burial, two modern analogues were collected to assess bleaching characteristics. One was from active bedload material being transported (MM1-1) and one from a recently deposited point bar (MM2-1) (Fig. 1C). While the sediments of the contemporary system are not necessarily representative of past conditions, they provide a modern baseline for assessment of the resetting of the OSL signal. Table 1 provides a summary of the depositional environment represented by each sample.

Luminescence dating

For OSL dating, equivalent dose (D_e) values were estimated for individual ~200-μm-diameter grains of quartz, using standard Risø single-grain aluminium discs (Bøtter-Jensen *et al.*, 2000) and a single-aliquot regenerative-dose procedure (SAR; Murray and Wintle, 2000). A full description of the OSL measurement and analytical procedures, including dose recovery and preheat plateau tests (i.e. Tables S1 and S2, Figs. S1–S9) are provided in the Supporting Information. Between 1000 and 2000 grains were measured for each sample (Table S2), and standard rejection criteria (e.g. Jacobs *et al.*, 2006) were applied to eliminate aberrant grains from final D_e determinations. Single grain D_e distributions were assessed based on their shape and the degree of overdispersion, considering variability in the intrinsic behaviour of grains and an understanding of the sedimentary context. The latter provide information about pre-depositional bleaching and post-depositional mixing as well as the potential effects of other factors, such as beta micro-dosimetry.

D_e values for TL dating (11 samples) were estimated from multi-grain aliquots of purified quartz grains (each ~100 μm in diameter) that were loaded onto aluminium discs as a monolayer; each aliquot contained between ~5000 and 9000 grains. D_e values were estimated using a combined regenerative and additive-dose protocol following Shepherd and Price (1990) and Nanson *et al.* (1991). For the regenerative-dose procedure, sample material was bleached under an ultraviolet light lamp (Philips MLU 300 W) for at least 24 h.

The effective dose rate for the analysed quartz grains is derived from gamma rays, beta particles, internal alpha particles and cosmic rays. Dose rates were measured independently for OSL and TL dating in the respective laboratories, using two separate sub-samples of the same homogenized sample material. Details regarding different methods and measurement procedures are provided in the Supporting Information. The same long-term water content estimates were used for both OSL and TL dating to correct the

Table 1. Overview of analysed samples. Depositional environment, location code, coordinates and the collection methods used for all samples are shown. Further details are presented in the Supporting Information.

OSL sample code	Location code	Depth (m)	Collection method*	Sediment†	Coordinates	Depositional environment
Sample set 1: Modern Murrumbidgee River – fluvial						
UoW1295	MM1-1	0	A	CS	55H 408489 6174299	Active bedload of current river channel, submerged at time of sample collection
UoW1313	MM2-1	0.20	B	MS	55H 406148 6174997	Point bar of current river, trough cross bedding, exposed at time of sample collection
Sample set 2: Yanco system – fluvial						
UoW1520	YA1-1	4.24	C	MS	55H 430673 6129183	Palaeochannel belt, channel deposit
UoW1590	YA1-1	5.10	C	CS	55H 430673 6129183	Palaeochannel belt, channel deposit
UoW1521	YA1-1	6.72	C	CS	55H 430673 6129183	Palaeochannel belt, channel deposit
UoW1488	YA2-1	2.50	B	CS	55H 403282 6109524	Palaeochannel belt, laterally accreted sediment, exposed in excavated pit
UoW1487	YA3-1	2.00	B	CS	55H 302670 6100790	Palaeochannel belt, laterally accreted sediment, exposed in excavated pit
UoW1522	YA4-1‡	2.12	C	CS	55H 273687 6111596	Palaeochannel belt, channel deposit
UoW1523	YA4-1‡	3.77	C	MS	55H 273687 6111596	Palaeochannel belt, channel deposit
UoW1591	YA4-2‡	7.64	C	MS	55H 273778 6111304	Palaeochannel belt, scroll bar ridge sediment
UoW1551	YA4-2‡	9.92	C	MS	55H 273778 6111304	Palaeochannel belt, scroll bar ridge sediment
UoW1553	YA4-3‡	2.26	C	FS	55H 273842 6111072	Palaeochannel belt, scroll bar swale sediment
UoW1552	YA4-3‡	5.01	C	CS	55H 273842 6111072	Palaeochannel belt, scroll bar swale sediment
UoW1554	YA4-3‡	14.01	C	CS	55H 273842 6111072	Palaeochannel belt, scroll bar swale sediment
Sample set 3: Yanco system – aeolian						
UoW1550	YA4-2	0.86	C	MS	55H 273778 6111304	Marginal dune, on scroll bar ridge, partly vegetated
Sample set 4: Gum Creek system – fluvial						
UoW1306	GC1-1	4.55	D	MS	55H 443015 6170249	Palaeochannel belt, channel deposit
UoW1483	GC2-1‡	5.79	C	FS	55H 410384 6169315	Palaeochannel belt, channel deposit
UoW1310	GC2-2‡	4.95	D	M	55H 410504 6169428	Palaeochannel belt, scroll bar ridge sediment
UoW1309	GC2-2‡	5.25	D	FS	55H 410504 6169428	Palaeochannel belt, scroll bar ridge sediment
UoW1555	GC2-3‡	2.19	C	FS	55H 410719 6169836	Palaeochannel belt, scroll bar ridge sediment
UoW1484	GC2-3‡	8.31	C	FS	55H 410719 6169836	Palaeochannel belt, scroll bar ridge sediment
UoW1485	GC2-4‡	7.48	C	G	55H 410840 6170091	Palaeochannel belt, scroll bar ridge sediment
UoW1486	GC2-4‡	11.28	C	MS	55H 410840 6170091	Palaeochannel belt, scroll bar ridge sediment
UoW1390	GC3-1	4.65	C	FS	55H 403677 6174325	Palaeochannel belt, channel deposit
UoW1389	GC3-1	4.95	C	CS	55H 403677 6174325	Palaeochannel belt, channel deposit
UoW1315	GC4-1	3.81	C	FS	55H 392657 6173320	Palaeochannel belt, channel deposit
UoW1391	GC4-1	6.75	C	CS	55H 392657 6173320	Palaeochannel belt, channel deposit
UoW1314	GC5-1	4.05	C	FS	55H 388244 6175049	Palaeochannel belt, channel deposit
UoW1322	GC5-1	5.85	C	CS	55H 388244 6175049	Palaeochannel belt, channel deposit
UoW1308	GC5-2	6.00	D	M	55H 388001 6175124	Palaeochannel belt, top of bank
UoW1307	GC6-1	2.00	B	MS	55H 318605 6183780	Palaeochannel belt, lateral accretion, exposed by cut bank of current river

Table 1. (*Continued*)

OSL sample code	Location code	Depth (m)	Collection method*	Sediment†	Coordinates	Depositional environment
Sample set 5: Gum Creek system – aeolian						
UoW1556	GC2-5	2.30	D	MS	55H 411239 6170812	Marginal dune, on scroll bar ridge, vegetated
UoW1557	GC5-3	3.25	D	MS	55H 388188 6175376	Marginal dune, on floodplain, vegetated

*A, grab sample; B, tube sample; C, sonic drill rig sample; D, percussion corer sample.
†G, gravel; CS, coarse sand; MS, medium sand; FS, fine sand; M, mud.
‡The location code of each core, along a transect, increases with distance to the channel.

beta, gamma and cosmic-ray dose rates. We used the current measured field water contents, which range between ~2 and 30% (Table 2), except for those samples collected from excavated pits and bank exposures (Table 1). For these samples, we used the average field value calculated from core samples of the same sample set and depositional context (Table 2). A relative uncertainty of ±25% (1σ) was assigned to each estimate of water content for OSL samples and an absolute error of ±3% (1σ) for TL samples. For the modern bedload sediments (UoW1295) we have estimated the saturated water content in the laboratory by filling pore volume to a maximum.

Results

Single-grain OSL dating

Table 3 contains information about the number of grains used for D_e determination, the D_e overdispersion (OD) values and the modelled D_e estimates used to calculate OSL ages. Between 2 and 20% of grains per sample were accepted for final D_e determination (Table S2). A typical OSL decay and dose–response curve for an accepted grain is shown in Fig. 4. General information about the OSL decay and dose–response behaviour is provided in the Supporting Information, together with details about why grains were rejected for all samples.

D_e values for all accepted grains are shown as radial plots for a representative sample from each sample set in Fig. 5 and for all samples in Figs. S5–S9. Sample sets 1 and 3 represent modern or near-modern fluvial and aeolian samples, respectively. Their radial plots are centred on 0 Gy and individual D_e values are shown as unlogged values (Fig. 5A,B,D). All three samples show similar patterns and ranges in D_e values: −1–5.3 Gy (UoW1295), −2.9–6.9 Gy (UoW1313) and −1.4–6.4 Gy (UOW1550). Only a small number of D_e values (3.3, 5.7 and 2.1%, respectively) range between ~2 and 6 Gy; the rest are statistically consistent with 0 Gy. Weighted mean D_e values of 0.19 ± 0.03, 0.45 ± 0.07 and 0.03 ± 0.07 Gy were calculated using the unlogged central age model (CAMul), showing no clear evidence for partial bleaching of the OSL signal in either fluvial or aeolian sediments.

Sample sets 2 and 4 make up most samples in this study ($n = 28$) and represent fluvial deposits associated with the two palaeochannel systems. Two types of D_e distributions were observed for these samples. The first type ($n = 23$) shows no distinct D_e distribution patterns (Figs. S6 and S8). OD values range between 24 ± 3 and 38 ± 3% (sample set 2) and 23 ± 2% and 43 ± 4% (sample set 4); there is a single sample (UoW1553) that gave a higher OD value of 51 ± 4%. We propose that the higher OD values are a combination of grain-to-grain differences in OSL behaviour, younger intrusive grains introduced by bioturbation (caused by soil microfauna and flora), and/or the general effects of pedogenesis (i.e. mottling and formation of iron coatings on grains) resulting in small-scale differences in the beta dose rate delivered to individual grains. Post-depositional pedogenesis and bioturbation are readily observed in the stratigraphic context of some samples presented in this study. Similar OD values (36 ± 3 and 37 ± 3%) and D_e distribution patterns were also observed for aeolian samples from the Gum Creek system (sample set 5), which are thought to have been sufficiently bleached in a bright setting like Australia (Figs. 5F and S9). For sample sets 2, 4 and 5 we have used the CAM (Galbraith *et al.*, 1999) for D_e determination, based on similarities in the shape and OD of D_e distributions, a lack of evidence for partial bleaching of modern sediments and our understanding of the sedimentological context of the samples.

A second type of D_e distribution ($n = 5$) was found for samples UoW1554 (Fig. S6: sample set 2), and UoW1308, 1483, 1486 and 1555 (Fig. S8: sample set 4). A large proportion of grains (47–78%) in each sample were either saturated with respect to dose or showed Class 3 grain behaviour (Table S2). Example decay and dose–response curves for two such grains are shown in Fig. S3. The D_e distributions can best be interpreted as truncated on the higher end of the D_e distribution, and only a minimum D_e value can be calculated with asymmetrical errors that are infinite in one direction. Minimum D_e values for these samples are based on the minimum age model (MAM) (Galbraith *et al.*, 1999). The D_e distributions of UoW1555 and UoW1308 are further complicated by the presence of younger intrusive grains, so D_e values for these samples are interpreted with caution.

Environmental dose rate details are provided in Table 2. The total dose rates for samples from the Yanco system range between 1.25 ± 0.05 and 2.95 ± 0.14 Gy ka^{-1}. A similar range (0.98 ± 0.04 to 3.05 ± 0.11 Gy ka^{-1}) was obtained for samples from the Gum Creek system.

Particular attention was given to samples UoW1523 and UoW1551 that had significantly lower gamma dose rate values compared to other samples from sample set 2. Additional inductively coupled plasma-mass spectrometry (ICP-MS) measurements were obtained, and measurement results are statistically consistent at 1σ between the two methods; ratios of gamma and beta dose rates of 1.06 ± 0.08 and 1.07 ± 0.07 (UoW1523) and 1.00 ± 0.07 and 1.04 ± 0.08 (UoW1551) were obtained.

Final single-grain OSL ages are listed in Table 3, together with the supporting D_e and dose rate estimates. Uncertainties on the ages are given at 1σ (standard error on the mean) and were derived by adding, in quadrature, all known and estimated sources of systematic and random errors. For the sample D_e value, the random error was obtained from the CAM or three-parameter MAM ($\sigma_b = 15$%). A systematic error of 2% was included for any possible bias associated with calibration of the laboratory beta-source. The total uncertainty

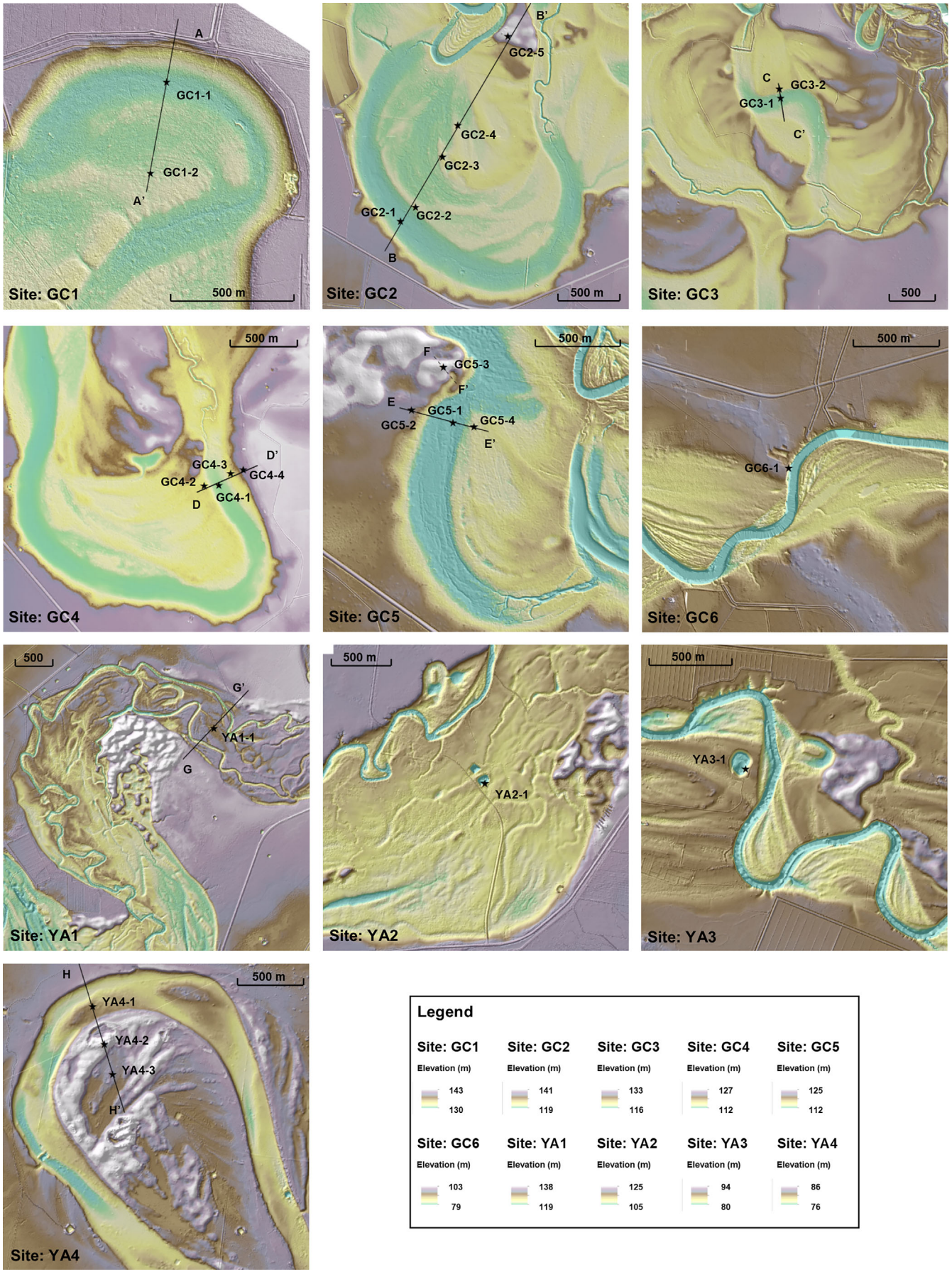

Figure 2. Digital elevation models (DEMs) of sampling sites. Sample locations are indicated with stars and transects as lines. [Colour figure can be viewed at wileyonlinelibrary.com].

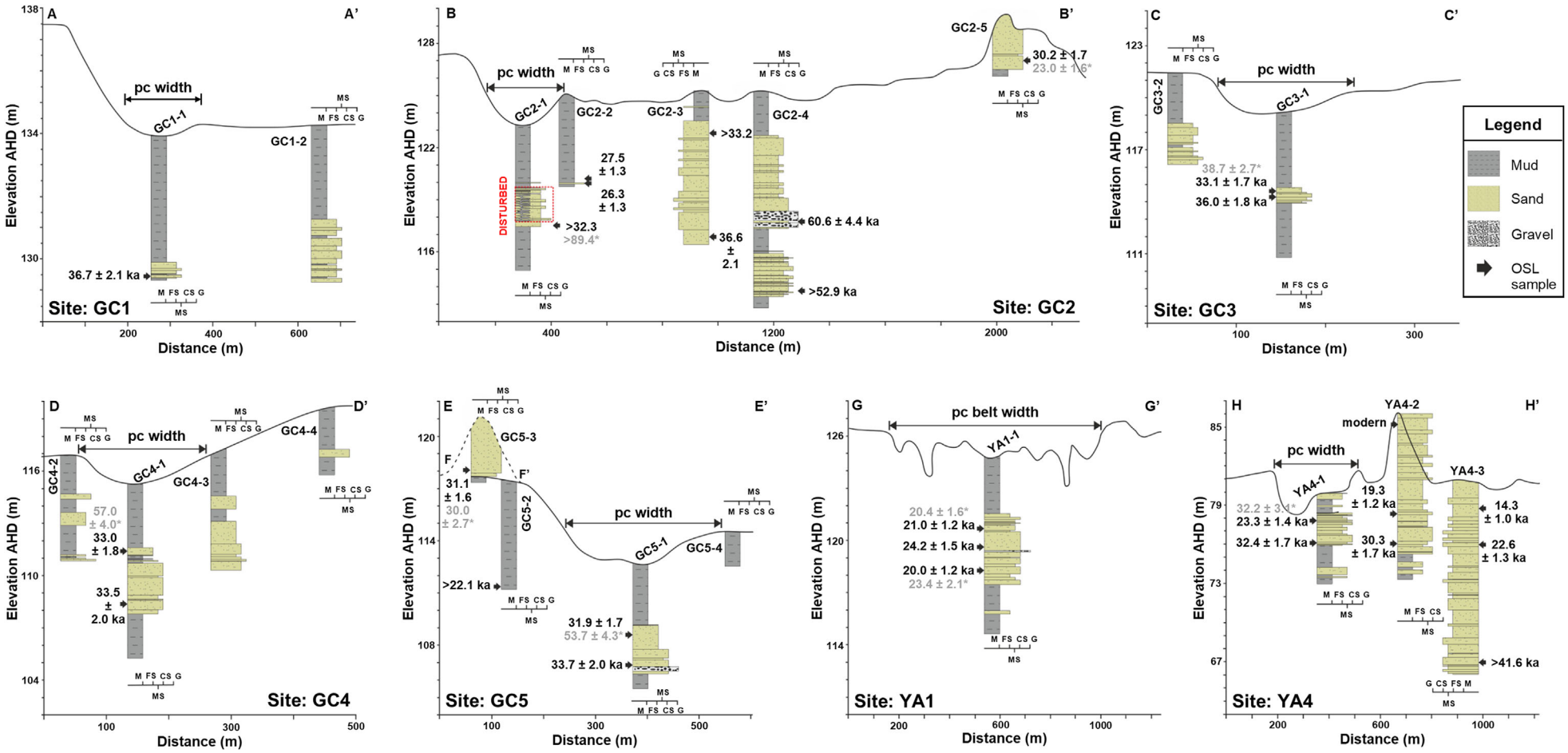

Figure 3. Cross-sections, core logs and OSL sample locations for all drill sites. OSL ages (black) and TL ages (grey with asterisk) are given next to each sample location. For locations of cross-sections see Fig. 2. [Colour figure can be viewed at wileyonlinelibrary.com].

Table 2. Environmental dose rate results for all OSL samples.

OSL sample code	Water content (%)†	Radionuclide concentrations			Dose rate			Total dose rate (Gy ka^{-1})
		U (ppm)	Th (ppm)	K (%)	Beta (Gy ka^{-1})	Gamma (Gy ka^{-1})	Cosmic (Gy ka^{-1})	
Sample set 1: Modern Murrumbidgee River – fluvial								
UoW1295	30 ± 5	0.69 ± 0.04	2.82 ± 0.34	1.12 ± 0.05	0.68 ± 0.04	0.37 ± 0.02	0.16 ± 0.02	1.23 ± 0.05
UoW1313	10 ± 5	1.17 ± 0.05	3.12 ± 0.45	2.27 ± 0.08	1.59 ± 0.10	0.76 ± 0.05	0.19 ± 0.03	2.56 ± 0.12
Sample set 2: Yanco system – fluvial								
UoW1520*	18 ± 4	0.95 ± 0.05	3.23 ± 0.46	1.99 ± 0.08	1.30 ± 0.07	0.63 ± 0.04	0.11 ± 0.03	2.06 ± 0.09
UoW1590	16 ± 4	0.77 ± 0.05	3.14 ± 0.43	1.72 ± 0.07	1.14 ± 0.06	0.56 ± 0.03	0.10 ± 0.03	1.82 ± 0.08
UoW1521*	12 ± 3	1.23 ± 0.06	3.75 ± 0.53	1.80 ± 0.07	1.29 ± 0.06	0.67 ± 0.04	0.10 ± 0.03	2.08 ± 0.08
UoW1488*	15 ± 4	1.02 ± 0.06	3.97 ± 0.54	1.33 ± 0.06	0.96 ± 0.05	0.54 ± 0.04	0.14 ± 0.03	1.67 ± 0.07
UoW1487	15 ± 4	1.07 ± 0.05	3.60 ± 0.49	1.32 ± 0.06	0.96 ± 0.05	0.53 ± 0.03	0.16 ± 0.02	1.67 ± 0.07
UoW1522*	16 ± 4	1.38 ± 0.07	4.08 ± 0.58	1.99 ± 0.08	1.38 ± 0.08	0.72 ± 0.04	0.16 ± 0.02	2.27 ± 0.09
UoW1523	16 ± 4	0.63 ± 0.03	2.07 ± 0.30	1.06 ± 0.05	0.72 ± 0.04	0.37 ± 0.02	0.14 ± 0.01	1.25 ± 0.05
UoW1591	22 ± 5	2.72 ± 0.17	12.01 ± 1.51	2.17 ± 0.11	1.69 ± 0.11	1.14 ± 0.09	0.11 ± 0.02	2.95 ± 0.14
UoW1551	13 ± 3	0.63 ± 0.04	2.47 ± 0.34	1.09 ± 0.05	0.77 ± 0.04	0.40 ± 0.02	0.10 ± 0.02	1.30 ± 0.05
UoW1553	18 ± 5	2.49 ± 0.11	6.43 ± 0.92	2.22 ± 0.10	1.64 ± 0.10	0.95 ± 0.06	0.15 ± 0.02	2.75 ± 0.12
UoW1552	20 ± 5	2.52 ± 0.13	7.95 ± 1.10	2.06 ± 0.10	1.56 ± 0.09	0.97 ± 0.07	0.13 ± 0.02	2.67 ± 0.12
UoW1554	12 ± 3	1.21 ± 0.05	2.17 ± 0.37	1.32 ± 0.06	0.97 ± 0.05	0.50 ± 0.03	0.08 ± 0.01	1.57 ± 0.06
Sample set 3: Yanco system – aeolian								
UoW1550	14 ± 3	1.58 ± 0.07	4.00 ± 0.59	1.66 ± 0.07	1.24 ± 0.06	0.68 ± 0.04	0.17 ± 0.03	2.11 ± 0.08
Sample set 4: Gum Creek system – fluvial								
UoW1306	23 ± 6	2.36 ± 0.10	4.90 ± 0.75	1.86 ± 0.09	1.33 ± 0.09	0.77 ± 0.05	0.13 ± 0.02	2.24 ± 0.10[A]
UoW1483*	15 ± 4	1.84 ± 0.09	6.09 ± 0.81	1.33 ± 0.07	1.10 ± 0.06	0.96 ± 0.06	0.11 ± 0.04	2.19 ± 0.09[B]
UoW1310	11 ± 3	3.27 ± 0.17	11.44 ± 1.47	1.76 ± 0.11	1.68 ± 0.08	1.21 ± 0.08	0.14 ± 0.02	3.05 ± 0.11[A]
UoW1309	7 ± 2	1.84 ± 0.14	11.79 ± 1.27	1.86 ± 0.10	1.65 ± 0.07	1.14 ± 0.07	0.14 ± 0.02	2.95 ± 0.10[A]
UoW1555	15 ± 4	1.80 ± 0.08	4.68 ± 0.69	1.71 ± 0.08	1.27 ± 0.07	0.73 ± 0.05	0.16 ± 0.02	2.20 ± 0.09
UoW1484	18 ± 5	1.58 ± 0.08	5.06 ± 0.67	1.63 ± 0.07	1.19 ± 0.07	0.69 ± 0.05	0.11 ± 0.02	2.00 ± 0.08
UoW1485	16 ± 4	0.84 ± 0.03	1.59 ± 0.27	0.74 ± 0.04	0.55 ± 0.03	0.30 ± 0.02	0.11 ± 0.02	0.98 ± 0.04
UoW1486	11 ± 3	1.27 ± 0.07	4.72 ± 0.64	1.05 ± 0.06	0.88 ± 0.04	0.56 ± 0.04	0.10 ± 0.01	1.55 ± 0.06
UoW1390*	16 ± 4	1.58 ± 0.09	5.42 ± 0.75	1.82 ± 0.08	1.33 ± 0.07	0.76 ± 0.05	0.13 ± 0.02	2.24 ± 0.09
UoW1389	14 ± 3	1.50 ± 0.06	3.16 ± 0.50	1.29 ± 0.06	0.99 ± 0.05	0.56 ± 0.03	0.14 ± 0.02	1.70 ± 0.07
UoW1315*	16 ± 4	2.57 ± 0.11	5.25 ± 0.81	1.65 ± 0.08	1.33 ± 0.07	0.81 ± 0.05	0.15 ± 0.02	2.30 ± 0.09
UoW1391	16 ± 4	1.08 ± 0.05	3.19 ± 0.45	0.82 ± 0.05	0.65 ± 0.04	0.41 ± 0.03	0.12 ± 0.02	1.20 ± 0.05
UoW1314*	18 ± 4	2.27 ± 0.09	5.27 ± 0.75	2.11 ± 0.09	1.54 ± 0.09	0.86 ± 0.05	0.14 ± 0.02	2.56 ± 0.11
UoW1322	11 ± 3	1.29 ± 0.07	4.07 ± 0.58	1.15 ± 0.06	0.93 ± 0.05	0.56 ± 0.03	0.13 ± 0.02	1.64 ± 0.06
UoW1308	13 ± 3	3.68 ± 0.17	9.75 ± 1.37	1.27 ± 0.09	1.36 ± 0.07	1.04 ± 0.07	0.13 ± 0.02	2.55 ± 0.10
UoW1307*	16 ± 4	1.61 ± 0.07	4.12 ± 0.62	1.36 ± 0.07	1.04 ± 0.06	0.61 ± 0.04	0.16 ± 0.02	1.82 ± 0.07
Sample set 5: Gum Creek system – aeolian								
UoW1556*	6 ± 2	1.41 ± 0.06	3.15 ± 0.49	1.91 ± 0.08	1.46 ± 0.06	0.74 ± 0.03	0.14 ± 0.03	2.36 ± 0.08
UoW1557*	2 ± 1	1.66 ± 0.06	3.37 ± 0.51	2.07 ± 0.08	1.68 ± 0.07	0.84 ± 0.04	0.14 ± 0.03	2.68 ± 0.08

*Samples were also dated using TL multi-grain dating and results are presented in Table 4.
†25% relative errors are assigned.
[A]Sample was bordering the mud base and channel infill, so a mix of those units and the investigated unit was used for the dosimetry sample.
[B]Sample was overlying the mud base, so 50% of the gamma dose rate was constituted by the underlying unit; radionuclide concentrations are reported for the sample unit.

on the dose rate was obtained as the quadratic sum of all random and systematic errors associated with the beta, gamma and cosmic-ray dose rates.

Finite age estimates were obtained for all but one (UoW1554) of the samples collected from the Yanco system (Table 3). The two Yanco sites investigated in detail show contrasting sub-surface sedimentology and surface morphology. At YA1 fine-grained channel fill overlies the former bedload (consisting of 2–3 m of coarse channel sand, Figs. 2 and 3) and shows consistency in age, ranging between 20.0 ± 1.2 and 24.2 ± 1.5 ka. Site YA4 shows more complex surface morphology and sub-surface sedimentology with an abandoned channel and a preserved scroll bar sequence with small aeolian dunes on the abandoned scroll bars (Fig. 3). The uppermost channel sands from YA4-1 yielded an age of 23.3 ± 1.4 ka and samples from equivalent elevations at YA4 across the transect are dated to 19.3 ± 1.2 and 14.3 ± 1.0 ka (Figs. 2 and 3). In contrast, lower in the channel sand sequence samples yielded ages that ranged from 22.6 ± 1.3 to 32.4 ± 1.7 ka. A significantly older minimum age of >41.6 ka (UoW1554) was obtained from channel sands at 13 m below ground surface, well below the depth of the abandoned palaeochannel. A sample collected from the source-bordering dune at 0.86-m depth (UoW1550; site YA4; Figs. 2 and 3) returned an age that is consistent with it being recently deposited.

For the Gum Creek system, finite age estimates were obtained for all but four of the samples (Table 3). Finite ages of former bedload sediment samples that were collected across four sites (GC1, GC3–5; Figs. 2 and 3) range from 31.9 ± 1.7 to 36.7 ± 2.1 ka. A minimum age of >32.3 ka was obtained for one sample (GC2-1). These ages are uniformly older than similar deposits of the Yanco system. Scroll bar samples, collected along a transect (GC2; Figs. 2 and 3), gave ages that range from 26.3 ± 1.3 to 60.6 ± 4.4 ka, and show an increase in age with distance from the channel. A minimum age of >33.2 ka was calculated for UoW1555, but a finite

Table 3. Single-grain OSL results: total dose rate, equivalent dose (D_e), overdispersion (OD) values, and ages.

OSL sample code	Location code	Depth (m)	Number of accepted/measured grains	D_e (Gy)	OD (%)	Total dose rate (Gy ka^{-1})	Age (ka)	Age model[C]
Sample set 1: Modern Murrumbidgee River – fluvial								
UoW1295	MM1-1	0	164/1000	0.19 ± 0.03	–	1.23 ± 0.05	–	CAMul
UoW1313	MM2-1	0.20	174/1000	0.45 ± 0.07	–	2.56 ± 0.12	–	CAMul
Sample set 2: Yanco system – fluvial								
UoW1520*	YA1-1	4.24	101/2000	42.6 ± 1.7	30.6 ± 2.9	2.06 ± 0.09	21.0 ± 1.2	CAM
UoW1590	YA1-1	5.10	78/1000	44.0 ± 2.1	33.8 ± 3.3	1.82 ± 0.08	24.2 ± 1.5	CAM
UoW1521*	YA1-1	6.72	102/1000	41.7 ± 1.9	38.1 ± 3.3	2.08 ± 0.08	20.0 ± 1.2	CAM
UoW1488*	YA2-1	2.50	53/1000	41.6 ± 2.2	31.0 ± 4.0	1.67 ± 0.07	25.0 ± 1.8	CAM
UoW1487	YA3-1	2.00	79/1000	40.7 ± 2.1	37.0 ± 3.8	1.67 ± 0.07	24.4 ± 1.6	CAM
UoW1522*	YA4-1	2.12	89/1000	53.0 ± 2.3	30.5 ± 3.1	2.27 ± 0.09	23.3 ± 1.4	CAM
UoW1523	YA4-1	3.77	121/1000	40.4 ± 1.4	24.6 ± 2.2	1.25 ± 0.05	32.4 ± 1.7	CAM
UoW1591	YA4-2	7.64	81/1000	57.0 ± 2.4	27.3 ± 3.1	2.95 ± 0.14	19.3 ± 1.2	CAM
UoW1551	YA4-2	9.92	97/1000	39.2 ± 1.6	29.5 ± 2.7	1.30 ± 0.05	30.3 ± 1.7	CAM
UoW1553	YA4-3	2.26	94/1000	39.4 ± 2.4	50.9 ± 4.3	2.75 ± 0.12	14.3 ± 1.0	CAM
UoW1552	YA4-3	5.01	92/1000	60.3 ± 2.2	24.2 ± 2.5	2.67 ± 0.12	22.6 ± 1.3	CAM
UoW1554	YA4-3	14.01	22/1000	63.6 + inf./−19.4	–	1.57 ± 0.06	>41.6	MAM
Sample set 3: Yanco system – aeolian								
UoW1550	YA4-2	0.86	107/1000	0.30 ± 0.07	–	2.11 ± 0.08	0.14 ± 0.03	CAMul
Sample set 4: Gum Creek system – fluvial								
UoW1306	GC1-1	4.55	161/1000	82.5 ± 2.8	30.2 ± 2.2	2.24 ± 0.10[A]	36.7 ± 2.1	CAM
UoW1483*	GC2-1	5.79	41/1000	70.7 + inf./−14.2	–	2.19 ± 0.09[B]	>32.3	MAM
UoW1310	GC2-2	4.95	164/1000	83.8 ± 2.5	23.3 ± 1.9	3.05 ± 0.11[A]	27.5 ± 1.3	CAM
UoW1309	GC2-2	5.25	151/1000	77.7 ± 2.7	29.3 ± 2.2	2.95 ± 0.10[A]	26.3 ± 1.3	CAM
UoW1555	GC2-3	2.19	95/1000	50.7 + inf./−3.2	–	2.20 ± 0.09	>33.2	MAM
UoW1484	GC2-3	8.31	113/1000	73.3 ± 2.7	26.8 ± 2.5	2.00 ± 0.08	36.6 ± 2.1	CAM
UoW1485	GC2-4	7.48	81/1000	59.4 ± 3.4	43.1 ± 4.2	0.98 ± 0.04	60.6 ± 4.4	CAM
UoW1486	GC2-4	11.28	69/1000	82.0 + inf./−6.8	–	1.55 ± 0.06	>52.9	MAM
UoW1390*	GC3-1	4.65	169/1000	73.9 ± 2.3	26.4 ± 1.9	2.24 ± 0.09	33.1 ± 1.7	CAM
UoW1389	GC3-1	4.95	171/1000	61.1 ± 2.0	29.1 ± 2.1	1.70 ± 0.07	36.0 ± 1.8	CAM
UoW1315*	GC4-1	3.81	181/1000	76.0 ± 2.9	38.4 ± 2.4	2.30 ± 0.09	33.0 ± 1.8	CAM
UoW1391	GC4-1	6.75	122/1000	40.2 ± 1.7	36.0 ± 2.9	1.20 ± 0.05	33.5 ± 2.0	CAM
UoW1314*	GC5-1	4.05	202/1000	81.6 ± 2.8	35.9 ± 2.2	2.56 ± 0.11	31.9 ± 1.7	CAM
UoW1322	GC5-1	5.85	128/1000	55.2 ± 2.5	42.8 ± 3.2	1.64 ± 0.06	33.7 ± 2.0	CAM
UoW1308	GC5-2	6.00	91/1000	56.4 + inf./−3.7	–	2.55 ± 0.10	>22.1	MAM
UoW1307*	GC6-1	2.00	199/1000	80.4 ± 2.7	31.9 ± 2.1	1.82 ± 0.07	44.2 ± 2.3	CAM
Sample set 5: Gum Creek system – aeolian								
UoW1556*	GC2-5	2.30	109/1000	71.2 ± 3.2	37.0 ± 3.1	2.36 ± 0.08	30.2 ± 1.7	CAM
UoW1557*	GC5-3	3.25	128/1000	83.2 ± 3.5	36.1 ± 2.9	2.68 ± 0.08	31.1 ± 1.6	CAM

*Samples were also dated using TL multi-grain dating and results are presented in Table 4.
[A]Sample was bordering the mud base and channel infill, so a mix of those units and the investigated unit was used for the dosimetry sample.
[B]Sample was overlying the mud base, so 50% of the gamma dose rate was constituted by the underlying unit; radionuclide concentrations are reported for the sample unit.
[C]Age models by Galbraith *et al.* (1999): CAM = central age model (logged), CAMul = central age model (unlogged) and MAM = minimum age model (σ_b = 15%).

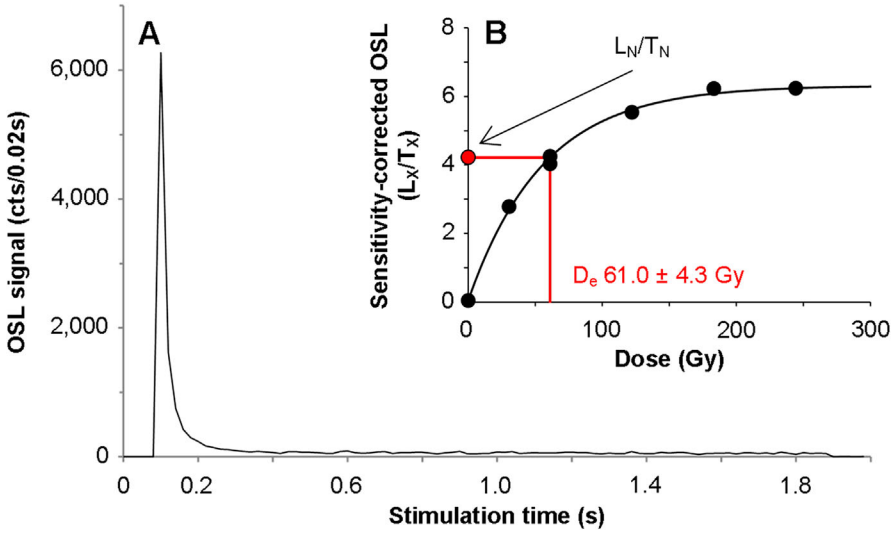

Figure 4. Typical OSL decay (**A**) and dose–response curve (**B**) for a single grain from sample UoW1314. The dose–response curve is constructed from the sensitivity-corrected OSL signals (L_X/T_X) following a range of different regenerative doses and fitted with a single saturating exponential function. The sensitivity-corrected natural signal (L_N/T_N) is projected onto the dose–response curve to obtain the D_e value in Gy by interpolation onto the dose axis. [Colour figure can be viewed at wileyonlinelibrary.com].

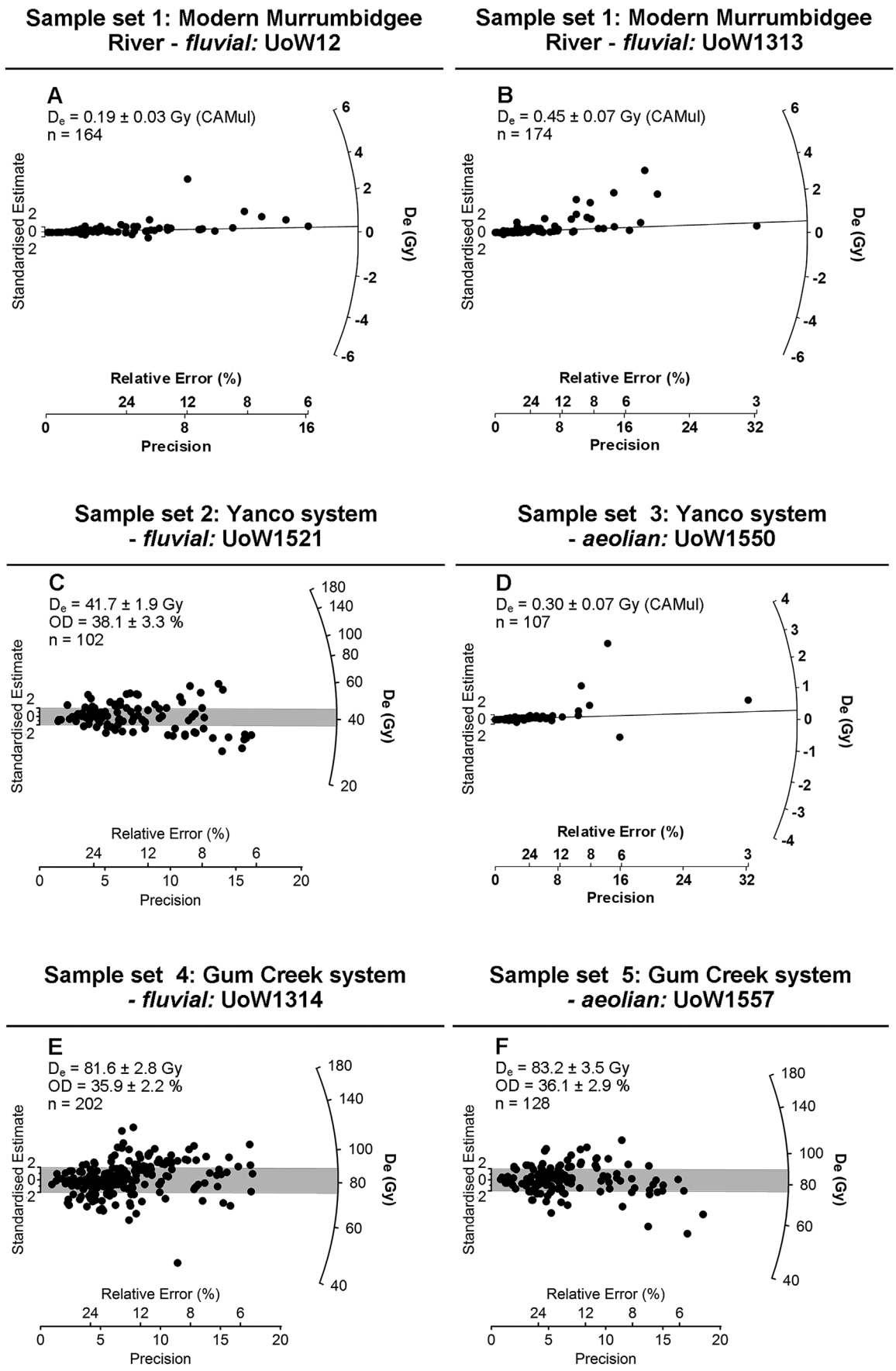

Figure 5. Radial plots of single-grain D_e distributions for a representative sample from each sample set. The radial plots in **A**, **B** and **D** are centred on 0 Gy and the grey lines are centred on the weighted mean D_e values determined using an unlogged version of the central age model. The radial plots and grey bands in **C**, **E** and **F** are centred on the weighted mean D_e value determined using the central age model. Radial plots for all samples are presented in the Supporting Information.

Table 4. Measurement results for all multi-grain TL samples.

TL sample code (OSL sample code)	Location code	Depth (m)	Water content (%)*	Radionuclide concentrations		Cosmic dose rate (Gy ka^{-1})	Total dose rate (Gy ka^{-1})	Plateau region (°C)	Analysis temperature (°C)	Number of accepted/measured discs	D_e (Gy)	Age (ka)
				U + Th (Bq kg^{-1})	K (%)							
Sample set 2: Yanco system – fluvial												
W4883 (UoW1520)	YA1-1	4.24	18 ± 3	29.44 ± 0.90	1.50 ± 0.05	0.11 ± 0.03	1.95 ± 0.05	300–500	375	(8/8)	40 ± 3	20.4 ± 1.6
W4884 (UoW1521)	YA1-1	6.72	12 ± 3	31.82 ± 0.92	1.42 ± 0.05	0.10 ± 0.03	2.01 ± 0.05	275–500	375	(8/8)	47 ± 4	23.4 ± 2.1
W4886 (UoW1488)	YA2-1	2.50	15 ± 3	28.54 ± 0.80	1.03 ± 0.05	0.14 ± 0.03	1.58 ± 0.05	257–500	375	(8/8)	42 ± 2	26.4 ± 1.5
W4885 (UoW1522)	YA4-1	2.12	16 ± 3	36.80 ± 1.00	1.44 ± 0.05	0.15 ± 0.03	2.09 ± 0.05	275–500	375	(8/8)	67 ± 6	32.2 ± 3.1
Sample set 4: Gum Creek system – fluvial												
W4853 (UoW1483)	GC2-1	5.79	15 ± 3	65.1 ± 1.8	1.03 ± 0.05	0.11 ± 0.04	2.21 ± 0.06	275–500	375	(8/8)	>197 ± 15	>89.4 ± 7.3
W4851 (UoW1390)	GC3-1	4.65	16 ± 3	44.6 ± 1.4	1.38 ± 0.05	0.12 ± 0.03	2.14 ± 0.05	275–500	375	(8/8)	83 ± 5	38.7 ± 2.7
W4849 (UoW1315)	GC4-1	3.81	16 ± 3	61.6 ± 1.3	1.33 ± 0.05	0.14 ± 0.03	2.41 ± 0.05	300–500	375	(8/8)	138 ± 9	57.0 ± 4.0
W4850 (UoW1314)	GC5-1	4.05	18 ± 3	64.4 ± 1.3	1.69 ± 0.05	0.13 ± 0.03	2.73 ± 0.05	275–500	375	(8/8)	146 ± 11	53.7 ± 4.3
W4852 (UoW1307)	GC6-1	2.00	16 ± 3	39.5 ± 1.2	1.09 ± 0.05	0.15 ± 0.03	1.81 ± 0.05	300–500	375	(8/8)	123 ± 9	68.0 ± 5.3
Sample set 5: Gum Creek system – aeolian												
W4813 (UoW1556)	GC2-5	2.30	6 ± 3	54.3 ± 1.5	1.67 ± 0.05	0.14 ± 0.03	2.87 ± 0.06	300–500	375	(8/8)	66 ± 4	23.0 ± 1.6
W4812 (UoW1557)	GC5-3	3.25	2 ± 3	45.5 ± 1.4	1.57 ± 0.05	0.14 ± 0.03	2.71 ± 0.06	300–500	375	(8/8)	82 ± 7	30.0 ± 2.7

*Absolute error values are assigned.

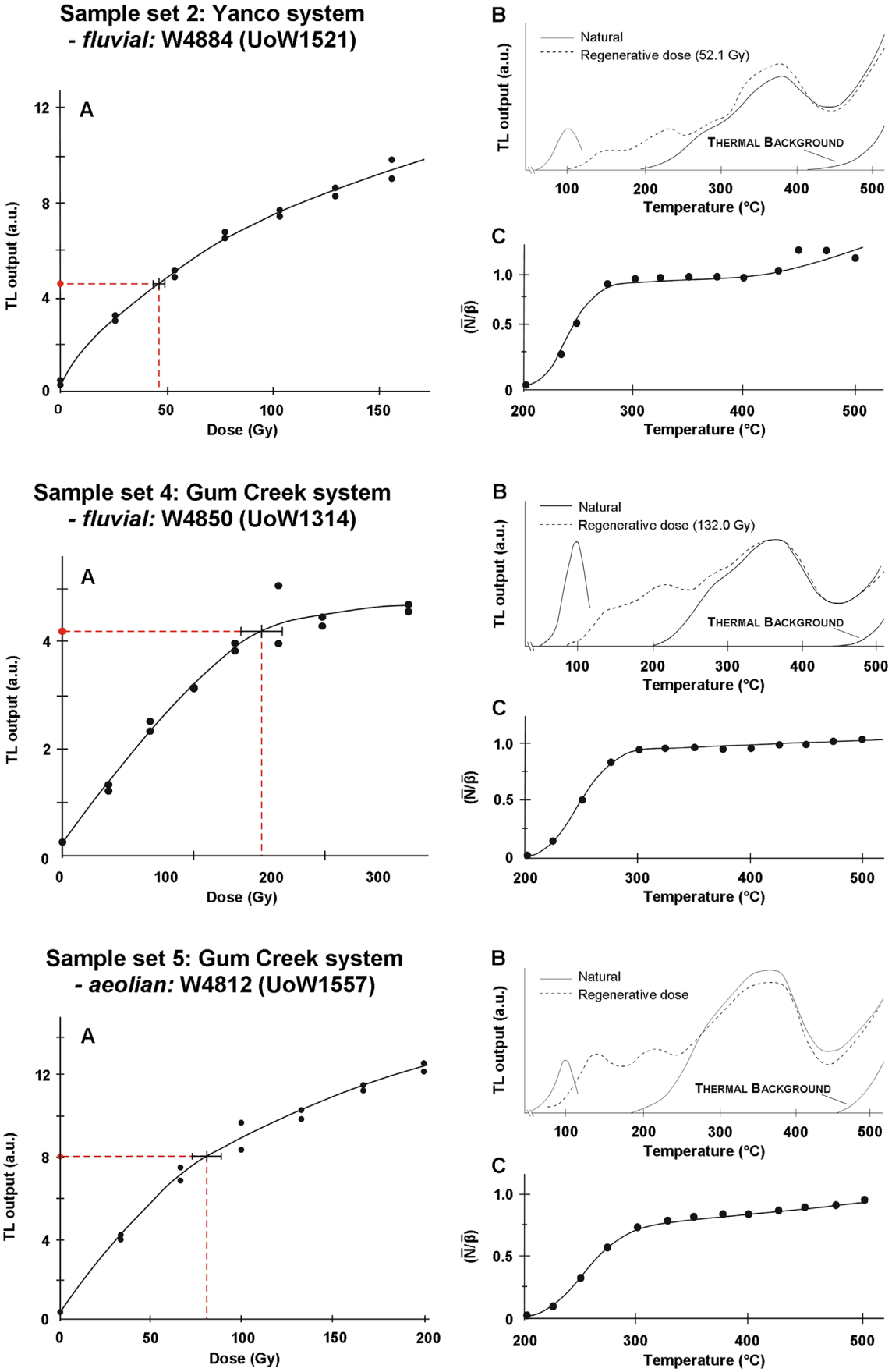

Figure 6. TL dose–response curves (**A**), glow curves (**B**) and temperature plateaus (**C**) for one representative sample of each sample set. [Colour figure can be viewed at wileyonlinelibrary.com].

age of 36.6 ± 2.1 ka was obtained for a sample ~6 m deeper from the same core (UoW1484). One sample (UoW1308) collected from a floodplain deposit (site GC5) gave a minimum age of >22.1 ka and another sample (UoW1307) collected from a laterally accreted deposit at the downstream site (GC6, Fig. 1) yielded a finite age of 44.2 ± 2.3 ka. The two samples taken from aeolian deposits at sites GC2 and GC5 (Figs. 2 and 3) gave consistent ages of 30.2 ± 1.7 and 31.1 ± 1.6 ka.

TL dating

The D_e values for each sample are provided in Table 4, together with the environmental dose rate results, and a representative glow curve, dose–response curve and temperature plateau are shown for a sample from each sample set in Fig. 6. Temperature plateaus were obtained from at least 280 to 450 °C (Fig. 6C), suggesting that both the 325 and 375 °C TL traps were emptied before deposition. Total dose rates for samples from the Yanco system range between 1.58 ± 0.05 and 2.09 ± 0.05 Gy ka^{-1}, and a similar range, but with slightly higher values, was obtained for the samples from the Gum Creek system: 1.81 ± 0.05 to 2.87 ± 0.06 Gy ka^{-1}. TL ages for samples from fluvial deposits of the Yanco system range between 20.4 ± 1.6 and 32.2 ± 3.1 ka. Four samples from fluvial deposits of the Gum Creek system gave TL ages between 38.7 ± 2.7 and 68.0 ± 5.3 ka. For one sample (W4853) a minimum age of >89.4 ka was obtained. The two samples from aeolian deposits associated with the Gum Creek system gave TL ages of 23.0 ± 1.6 and 30.0 ± 2.7 ka.

Discussion

Single-grain OSL and TL age comparisons

Fig. 7 shows a comparison of the TL and single-grain OSL ages obtained in this study. Only half of the samples measured using the two techniques are consistent at 2σ. All other TL ages are between 54 and 73% older than their corresponding OSL ages, except for UOW1556, an aeolian sample from the Gum Creek system, which is ~14% younger. A single sample (UoW1483) gave a minimum age using the two methods.

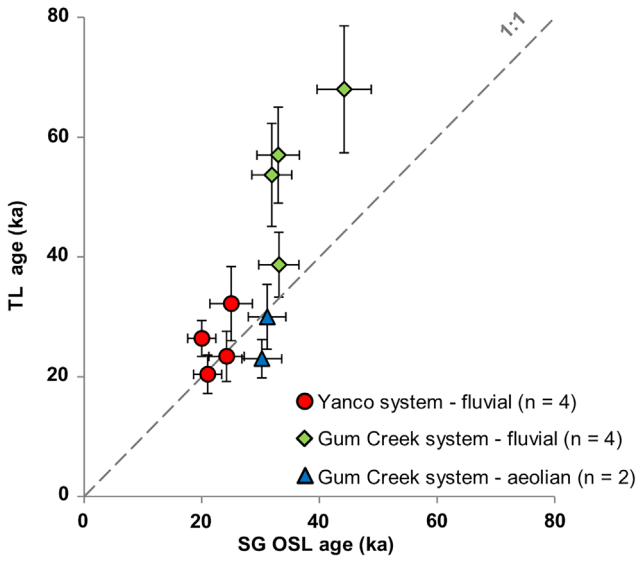

Figure 7. Age comparison for all samples measured using both multi-grain TL and single-grain OSL methods. Errors are shown at 2σ. [Colour figure can be viewed at wileyonlinelibrary.com].

Age overestimation is not due to partial bleaching of the TL signal. TL preheat plateaus extend from 280 to 450 °C (Fig. 6) that include the so-called hard-to-bleach signal (375 °C TL peak) (e.g. Aitken, 1985; Franklin *et al.*, 1995). To further explore potential reasons for the discrepant results, we compared the independently obtained radionuclide concentrations used in estimation of the OSL and TL ages, respectively. Fig. 8A compares the combined U and Th concentrations (TSAC; both studies). Values for individual samples obtained in the two laboratories are consistent at 2σ for seven of the 10 samples; UoW1314 (1.27 ± 0.09), UoW1556 (1.75 ± 0.13) and UoW1557 (1.30 ± 0.09) have ratios that are statistically inconsistent. Fig. 8B compares the K concentrations derived using atomic emission spectroscopy (AES; TL study) and a combination of TSAC and GM-25-5 beta counting (OSL study). None of the samples have K concentrations that are consistent between the two techniques; the AES-derived K values are systematically smaller (by ~24%). We verified the K values for samples in this

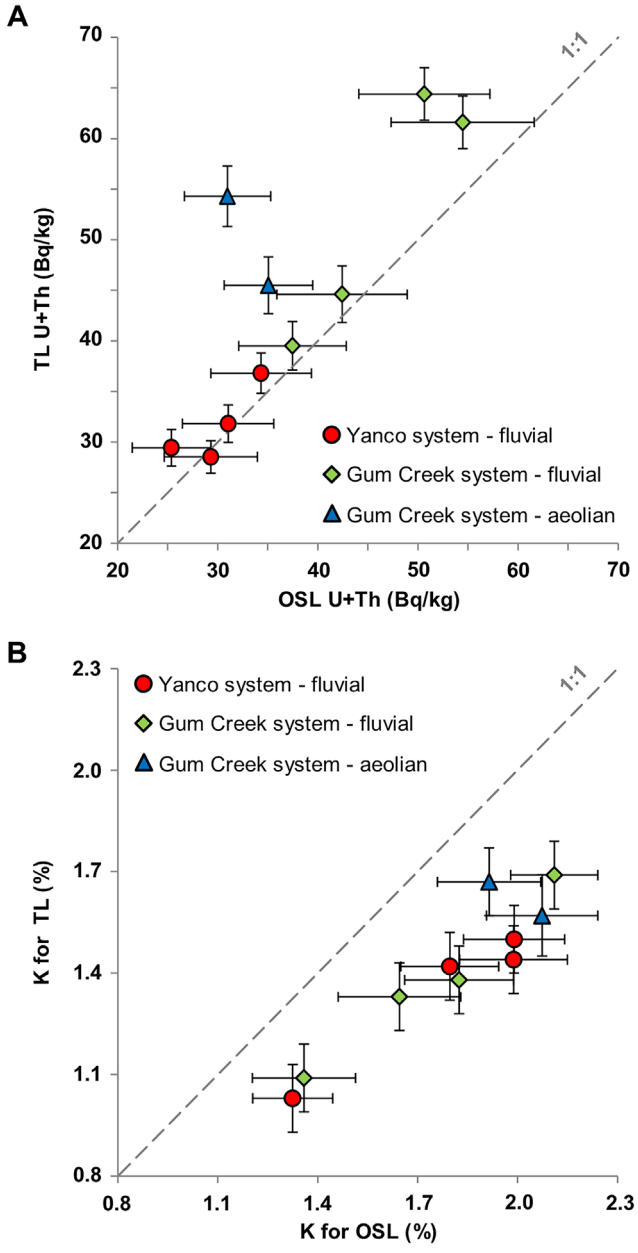

Figure 8. Radionuclide comparison of (**A**) combined uranium and thorium (Bq kg^{-1}) and (**B**) potassium (%) from measurements obtained in the OSL and TL laboratories. Errors are shown at 2σ. [Colour figure can be viewed at wileyonlinelibrary.com].

study with X-ray fluorescence (XRF). An average ratio of 0.99 ± 0.05 was obtained when compared with K concentrations derived from TSAC and GM-25-5 beta counting, and an average ratio of 0.78 ± 0.04 when compared to AES (Table S3). Note that all samples, including samples that showed good agreement between TL and OSL ages, have discrepant K values. Using the XRF-derived K values for the calculation of the TL ages, however, does not fully account for differences between TL and OSL ages. Further work is required to resolve the issue with AES-derived K values and other sources contributing to differences in age between the two techniques.

Revised chronology

We chose to use the single-grain OSL ages for the re-evaluation of when fluvial activity occurred on the Riverine Plain, because of the inherent benefits associated with measuring individual grains over multi-grain aliquots (e.g. Jacobs and Roberts, 2007; Roberts *et al.*, 2015) and our greater confidence in the dose rate values. To constrain phases of enhanced fluvial activity, only ages for samples collected from palaeochannel bedload deposits were included, thus excluding samples from adjacent scroll-bar sequences (Table 1). These bedload deposits represent the last time interval of channel activity and can be directly linked to palaeochannel morphology from which sediment and water discharge can be inferred. The bedload ages that were included in calculation of periods of enhanced fluvial activity are shown in red (Yanco phase) and green (Tombullen phase) in Fig. 9, with those excluded indicated in grey.

For the Gum Creek system, we refer to the period of enhanced fluvial activity as the Tombullen phase (Fig. 9). Defining the Tombullen phase allows separating ages obtained for samples contained within the Tombullen reach from those collected elsewhere along the Gum Creek palaeochannel system [i.e. GC6, UoW1307 (Fig. 1) or other TL ages of Page *et al.*, 1996]. Ages range between 36.7 ± 2.1 and 31.9 ± 1.7 ka ($n = 7$; Table 3 and green diamonds in Fig. 9). Enhanced fluvial activity, therefore, occurred sometime between 41 and 29 ka (2σ range of ages). The end of this phase is further suggested by two source-bordering dunes found along the Tombullen reach. These may mark the termination of fluvially sourced sediments that were available for re-deposition in aeolian dunes shortly after ~30 ka.

Not all sites in the Tombullen reach provide unambiguous results; some have mid-point ages that are both younger and older, but the ages are in most cases statistically consistent at 2σ with the age range obtained for the Tombullen phase. These include scroll bar sediments (GC2-2 and GC2-3; Tables 1 and 3) that yielded ages clustered around ~37 and ~27 ka and an age of 44.2 ± 2.3 ka for a laterally accreted deposit collected from a bank exposure downstream of the Tombullen reach at site GC6 (Fig. 1C). Only minimum ages could be obtained for two samples from in-channel deposits at site GC2 (Figs. 2 and 3), so their direct relationship with the channel in its preserved shape, and the association with the Tombullen phase, remains uncertain.

For the Yanco system, we call the period of enhanced fluvial activity the Yanco phase, following the terminology of Page *et al.* (1996). Ages for the Yanco phase range between 25.0 ± 1.8 and 20.0 ± 1.2 ka ($n = 6$; Table 3 and red circles in Fig. 9). Enhanced fluvial activity, therefore, occurred sometime between 29 and 18 ka (2σ range of ages). Palaeoscroll bars at site YA4 provide evidence of past lateral migration (Figs. 2 and 3) with three ages along a transect ranging between 23.3 ± 1.4 and 19.3 ± 1.2 ka. A lack of precision on individual ages, however, prevents calculation of migration rates at this location. Ages of 32.4 ± 1.7 and 30.3 ± 1.7 ka for samples from a former in-channel bedload unit and an adjacent scroll bar, respectively, are consistent with ages obtained for the Tombullen phase. These are thought to be indicators of fluvial activity down the Yanco Creek during the Tombullen phase with subsequent reoccupation of the site (YA4) during the Yanco phase.

Comparison with previous findings

Fig. 9 shows all finite OSL and TL ages obtained in this study together with TL ages obtained by Page *et al.* (1996) for the Gum Creek (Tombullen in this study; green diamonds) and Yanco phases (red circles). Page *et al.* (1996) has previously

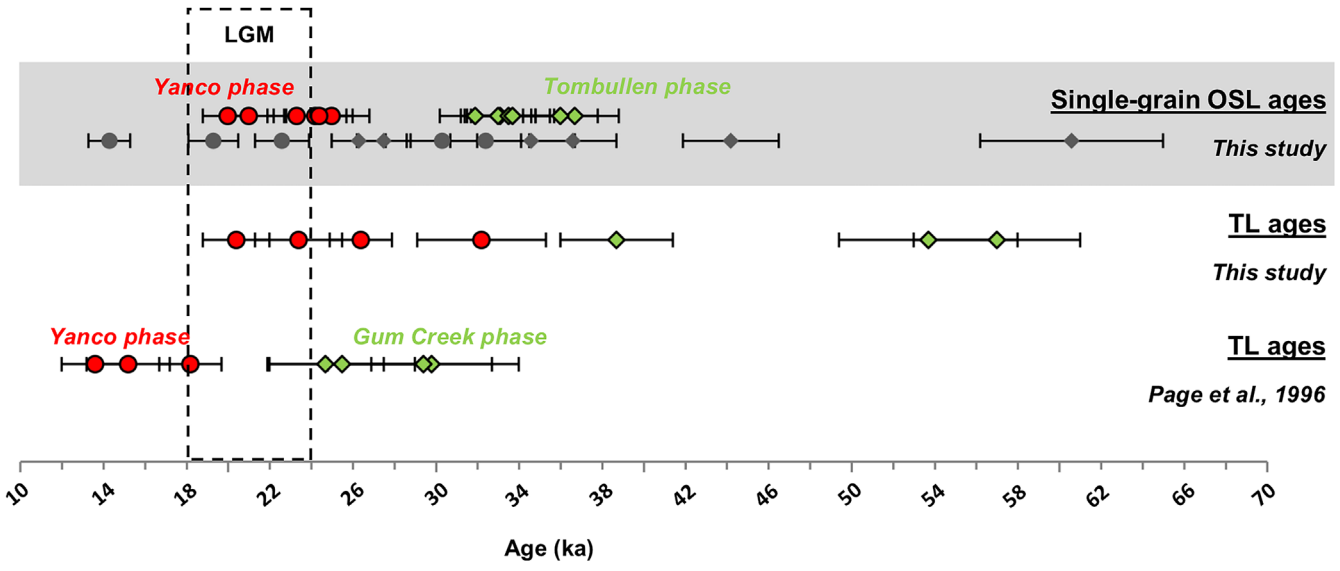

Figure 9. All finite single-grain OSL and multi-grain TL ages obtained for fluvial deposits in this study. Filled green diamonds show ages associated with bedload samples collected from the Gum Creek system and filled red circles samples from the Yanco system. OSL ages for fluvial deposits that are not used to distinguish phases of enhanced fluvial activity are presented in grey. Also shown are TL ages reported in Page *et al.* (1996). All ages are presented with 1σ errors. [Colour figure can be viewed at wileyonlinelibrary.com].

assigned periods of enhanced fluvial activity for the Gum Creek phase to 35–25 ka and the Yanco phase to 20–13 ka; both periods overlap with, but are systematically younger than, the ranges proposed in this study.

A number of sites investigated in this study were previously dated using TL, including samples from GC2 and GC6 in the Gum Greek system and from YA2, YA3 and YA4 in the Yanco system (Fig. 1C). Page *et al*. (1996) provide a full description of the TL sample locations. A comparison of the ages is provided in Table S4 where it can be seen that for all samples the TL ages presented by Page *et al*. (1996) are systematically younger than the corresponding new OSL ages. This is in contrast to the TL ages produced in the current study that were all systematically older and also more spread (Fig. 9). A key difference between the new OSL and old TL chronologies is the estimate of time-averaged water content used to calculate the environmental dose rates. Page *et al*. (1996) used water contents of 2–11% (weighted mean of 5.5%) for fluvial sediments, compared to 7–23% (weighted mean of 15%) in this study. If an average water content of 5.5% is used in this study, then the OSL ages will decrease by ~4 ka for the Tombullen phase and by ~2 ka for the Yanco phase. The differences in water content explain some but not all the differences between the OSL and TL ages. Regardless of choice of water content, OSL ages for the Yanco phase remain consistent with a period of enhanced fluvial activity throughout the LGM. This contradicts the original interpretation of Page *et al*. (1996) who suggested that rivers were less active during the LGM itself (Fig. 9). We also found no support for the 9 ka age obtained by Banerjee *et al*. (2002) who suggested on the basis of this single age that the Yanco phase extended into the Holocene.

Our results demonstrate enhanced fluvial activity, as recorded in large-dimension palaeochannels, from 41 to 18 ka, including at the peak of the LGM. There may be some weak statistical support for a period of reduced discharge at 30–25 ka (Fig. 9) or it may simply reflect deposition within another series of palaeochannels not investigated here. A reduced discharge at 30–25 ka contrasts with chronological interpretations from other river systems in the region. For example, on the Lachlan River (a tributary of the Murrumbidgee River; Fig. 1B), enhanced fluvial activity was thought to have occurred 34–20 ka, terminating with a period of decreased discharge at the peak of the LGM (OSL chronology; Kemp and Rhodes, 2010). Palaeochannel activity of the Goulburn River, which drains the catchment south of our study area (Fig. 1B), was linked to a period of enhanced fluvial activity that lasted 30–15 kyr (Bowler, 1978). In the Gwydir River (north of the Lachlan River), Pietsch *et al*. (2013) present phases of enhanced fluvial activity at 43–34 ka and 19–16 ka (OSL chronology) with a longer period of depressed flows from ~34 to 19 ka. These regional differences cannot currently be explained, but a systematic dating study coupled with palaeohydrological and palaeoenvironmental research in the southern Murray–Darling Basin should help to resolve some of these issues in the future.

Conclusions

In this study, we dated with single-grain OSL both fluvial and aeolian sediments of the modern Murrumbidgee River and its two palaeochannel systems – the Gum Creek and Yanco systems. We also measured a sub-set of samples with TL dating resulting in some discrepancies for reasons that are still not fully understood. Partial bleaching of the TL signal was discounted, but measurement of potassium was identified as one source of uncertainty. In addition, significant variations in moisture content between this study and earlier research by Page *et al*. (1996) could contribute to the differences in the identified periods of fluvial activity.

We based our revised chronology on the single grain OSL ages because of their internal consistency obtained for samples collected from bedload deposits, and our ability to ascertain in more detail why samples may vary from each other due to pre- and post-depositional effects. This new chronology suggests that periods of enhanced fluvial activity associated with increased sediment and water discharge occurred at 41–29 ka for the Tombullen phase and at ~29–18 ka for the Yanco phase. The latter phase is consistent with fluvial activity during the global LGM. Previous assumptions of diminished fluvial activity at the peak of the LGM and the absence of source-bordering dunes associated with the Gum Creek system (Page *et al*., 1996) have been revised. A more systematic geochronological approach is needed to determine the regional coherence of phases of enhanced fluvial activity in the Murray–Darling Basin. Forthcoming work applying the same dating methods to equivalent proxies in the other major tributaries along with palaeohydrological analyses will enable a more finely resolved assessment of the timing and magnitude of changes in runoff during the LGM.

Supporting Information

Details about the sampling methods and OSL and TL measurement methods and analytical results are provided in Sections S1, S2 and S3, respectively. A comparison of ages obtained in this study and by Page *et al*. (1996) is summarized in Section S4.

Figure S1 Dose–recovery test results for four representative samples. Measured/given dose ratios obtained using the preferred preheat temperature combinations are displayed as radial plots for individual grains.

Figure S2 Dose–recovery and preheat plateau test results for a representative fluvial sample from the Yanco and Gum Creek systems.

Figure S3 Representative dose decay and dose–response curve for grains that were saturated or exhibited Class-3 grain behaviour.

Figure S4 Decay curves, normalized decay curves and dose–response curves of an individual grain for a representative sample from each sample set.

Figures S5–S9 Single grain D_e values shown as radial plots together with the weighted mean D_e value, number of grains included in the final D_e value and OD values for all samples. Samples from the same sample sets are shown together.

Table S1 Dose–recovery and preheat plateau test results for four representative samples following a range of different preheat temperature combinations.

Table S2 Number of individual quartz grains measured, rejected and accepted for each sample, together with the reasons for grain rejection.

Table S3 Comparison of K (%) concentrations derived from three different methods.

Table S4 Comparison of TL ages presented in Page *et al*. (1996) with OSL ages presented in this study for samples from the same sites.

Acknowledgements. This research was funded through the Australian Research Council Discovery grant DP110103081 to Tim Cohen and James Shulmeister, as well as through a University Postgraduate Award from the University of Wollongong to Daniela Mueller. The authors thank the NSW National Parks and Wildlife Services for research permit SL101233 and sampling approval. Our appreciation goes to ANSTO and Patricia Gadd for allowing and supporting use of

their facility. We thank Ann Wintle for constructive criticism on the manuscript. Additionally, we would like to thank the landholders for permission and cooperation and Venera Espaňon, Rafael Carvalho, Yasaman Jafari and Terry Lachlan for their support in the field or laboratory.

Abbreviations. AES, atomic emission spectroscopy; CAM, central age model; DEM, digital elevation model; ICP-MS, inductively coupled plasma-mass spectrometry; LGM, Last Glacial Maximum; MAM, minimum age model; OD, overdispersion; OSL, optically stimulated luminescence; SAR, single-aliquot regenerative-dose procedure; TL, thermoluminescence; XRF, X-ray fluorescence.

References

Aitken MJ. 1985. *Thermoluminescence Dating*. Academic Press: London.

Banerjee DK, Page KJ, Lepper K. 2002. Optical dating of palaeochannel deposits in the Riverine Plain, Southeastern Australia: testing the reliability of existing thermoluminescence dates. *Radiation Protection Dosimetry* **101**: 327–332.

Bishop P, Godley D. 1994. Holocene palaeochannels at SiSatchanalai, north-central Thailand: ages, significance and palaeoenvironmental indications. *The Holocene* **4**: 32–41.

Bøtter-Jensen L, Bulur E, Duller GAT *et al*. 2000. Advances in luminescence instrument systems. *Radiation Measurements* **32**: 523–528.

Bowler JM, Johnston H, Olley JM *et al*. 2003. New ages for human occupation and climatic change at Lake Mungo, Australia. *Nature* **421**: 837–840.

Bowler JM. 1978 Quaternary climate and tectonics in the evolution of the Riverine Plain, Southeastern Australia. In: *Landform Evolution in Australasia*, Davies JL, Williams MA (eds). Australian National University: Canberra; 70–112.

Braconnot P, Harrison SP, Kageyama M *et al*. 2012. Evaluation of climate models using palaeoclimatic data. *Nature Climate Change* **2**: 417–424.

Brown CM, Stephenson AE. 1991. Geology of the Murray Basin, southeastern Australia. Vol. 235. Australian Government Publication Service: Canberra.

Butler BE. 1958. *Depositional Systems of the Riverine Plain of South-Eastern Australia in Relation to Soils, issue 10 of Soil Publications*. Commonwealth Scientific and Industrial Research Organization: Australia.

Butler BE. 1960. Riverine deposition during arid phases. *Australian Journal of Science* **22**: 451–452.

Coventry RJ. 1976. Abandoned shorelines and the late Quaternary history of Lake George, New South Wales. *Journal of the Geological Society of Australia* **23**: 249–273.

Dodson JR, Wright RVS. 1989. Humid to Arid to Subhumid Vegetation Shift on Pilliga Sandstone, Ulungra Springs, New South Wales. *Quaternary Research* **32**: 182–192.

Dury GH. 1976. Discharge prediction, present and former, from channel dimensions. *Journal of Hydrology* **30**: 219–245.

Franklin AD, Prescott JR, Scholefield RB. 1995. The mechanism of thermoluminescence in an Australian sedimentary quartz. *Journal of Luminescence* **63**: 317–326.

Geoscience Australia. 2011. 1 second SRTM Derived Digital Elevation Model, Commonwealth of Australia, dataset, DVD.

Galbraith RF, Roberts RG, Laslett GM *et al.* 1999. Optical dating of single and multiple grains of quartz from Jinmium rock shelter, Northern Australia: Part I, Experimental design and statistical models. *Archaeometry* **41**: 339–364.

Galloway RW. 1965. Late Quaternary climates in Australia. *The Journal of Geology* **73**: 603–618.

Green D, Petrovic J, Burrell M. 2011. *Water Resources and Management Overview: Murrumbidgee Catchment*. NSW Office of Water: Australia.

Harvey AM. 1969. Channel capacity and the adjustment of streams to hydrologic regime. *Journal of Hydrology* **8**: 82–98.

Hesse PP, Magee JW, van der Kaars S. 2004. Late Quaternary climates of the Australian arid zone: a review. *Quaternary International* **118–119**: 87–102.

Hickin EJ. 1977. The analysis of river-planform responses to changes in discharge. River channel changes. In *River Channel Changes*, Gregory KJ (ed.). John Wiley & Sons: Chichester; 249–263.

Hope J. 1983. Southern Australia at 18,000 B.P In: *Proceedings of the First CLIMANZ Conference, 1981*, Chappell J, Grindrod A (eds). Australian National University: Canberra; 57.

Jacobs Z, Duller GAT, Wintle AG. 2006. Interpretation of single grain D_e distributions and calculation of D_e. *Radiation Measurements* **41**: 264–277.

Jacobs Z, Roberts RG. 2007. Advances in optically stimulated luminescence dating of individual grains of quartz from archeological deposits. *Evolutionary Anthropology: Issues, News, and Reviews* **16**: 210–223.

Kaplan MR, Ackert, RP, Singer BS *et al*. 2004. Cosmogenic nuclide chronology of millennial-scale glacial advances during O-isotope stage 2 in Patagonia. *Geological Society of America Bulletin* **116**: 308–321.

Kemp J, Pietsch T, Gontz A *et al*. 2017. Lacustrine-fluvial interactions in Australia's Riverine Plains. *Quaternary Science Reviews* **166**: 352–362.

Kemp J, Rhodes EJ. 2010. Episodic fluvial activity of inland rivers in southeastern Australia: palaeochannel systems and terraces of the Lachlan River. *Quaternary Science Reviews* **29**: 732–752.

Langford-Smith T. 1959. Deposition on the Riverine Plain of South-Eastern Australia. *Australian Journal of Science* **22**: 73–74.

McCulloch RD, Fogwill CJ, Sugden DE *et al*. 2005. Chronology of the last glaciation in central Strait of Magellan and Bahía Inútil, southernmost South America. *Geografiska Annaler: Series A, Physical Geography* **87**: 289–312.

Mix AC, Bard E, Schneider R. 2001. Environmental processes of the ice age: land, oceans, glaciers (EPILOG). *Quaternary Science Reviews* **20**: 627–657.

Moreno PI, Lowell TV, Jacobson Jr GL *et al*. 1999. Abrupt vegetation and climate changes during the Last Glacial Maximumand Last Termination in the Chilean Lake District: a case study from Canal De La Puntilla (41°S). *Geografiska Annaler, Series A: Physical Geography* **81**: 285–311.

Murray AS, Wintle AG. 2000. Luminescence dating of quartz using an improved single-aliquot regenerative-dose protocol. *Radiation Measurements* **32**: 57–73.

Nanson GC, Price DM, Short SA *et al*. 1991. Comparative uranium–thorium and thermoluminescence dating of weathered Quaternary alluvium in the tropics of Northern Australia. *Quaternary Research* **35**: 347–366.

Page KJ, Nanson GC. 1996. Stratigraphic architecture resulting from Late Quaternary evolution of the Riverine Plain, south-eastern Australia. *Sedimentology* **43**: 927–945.

Page KJ, Nanson GC, Price DM. 1996. Chronology of Murrumbidgee River palaeochannels on the Riverine Plain, southeastern Australia. *Journal of Quaternary Science* **11**: 311–326.

Pels S. 1964. The present and ancestral Murray River system. *Australian Geographical Studies* **2**: 111–119.

Petherick L, Bostock HC, Cohen TJ *et al*. 2013. Climatic records over the past 30 ka from temperate Australia – a synthesis from the Oz-INTIMATE workgroup. *Quaternary Science Reviews* **74**: 58–77.

Pietsch TJ, Nanson GC, Olley JM. 2013. Late Quaternary changes in flow-regime on the Gwydir distributive fluvial system, southeastern Australia. *Quaternary Science Reviews* **69**: 168–180.

Reeves JM, Barrows TT, Cohen TJ *et al*. 2013. Climate variability over the last 35,000 years recorded in marine and terrestrial archives in the Australian region: an OZ-INTIMATE compilation. *Quaternary Science Reviews* **74**: 21–34.

Roberts RG, Jacobs Z, Li B *et al*. 2015. Optical dating in archaeology: thirty years in retrospect and grand challenges for the future. *Journal of Archaeological Science* **56**: 41–60.

Schumm SA. 1968. River adjustment to altered hydrological regimen – Murrumbidgee River and paleochannels, Australia. *United States Geological Survey Professional Paper* **598**.

Shepherd MJ, Price DM. 1990. Thermoluminescence dating of late Quaternary dune sand, Manawatu/Horowhenua area, New Zealand:

a comparison with ^{14}C age determinations. *New Zealand Journal of Geology and Geophysics* **33**: 535–539.

Shulmeister J, Goodwin I, Renwick J *et al.* 2004. The Southern Hemisphere westerlies in the Australasian sector over the last glacial cycle: a synthesis. *Quaternary International* **118–119**: 23–53.

Singh G, Geissler EA. 1985. Late Cainozoic history of vegetation, fire, lake levels and climate, at Lake George, New South Wales, Australia. *Philosophical Transactions of the Royal Society B: Biological Sciences* **311**: 379–447.

Williams GP. 1984. Paleohydrologic equations for rivers. In *Developments and Applications of Geomorphology*, Costa JE, Fleisher PJ (eds). Springer-Verlag: Berlin; 343–367.

Williams NJ, Harle KJ, Gale SJ *et al.* 2006. The vegetation history of the last glacial–interglacial cycle in eastern New South Wales, Australia. *Journal of Quaternary Science* **21**: 735–750.

Zhu J, Lücke A, Wissel H *et al.* 2014. Climate history of the Southern Hemisphere Westerlies belt during the last glacial–interglacial transition revealed from lake water oxygen isotope reconstruction of Laguna Potrok Aike (52° S, Argentina). *Climate of the Past* **10**: 2153–2169.